IEEE Sensors Council

Characterization of Hydrogenated Amorphous Silicon Sensors on Polyimide Flexible Substrate

Mauro Menichelli, Luca Antognini, Saba Aziz, Aishah Bashiri, Marco Bizzarri, Lucio Calcagnile, Mirco Caprai, Domenico Caputo, Anna Paola Caricato, Roberto Catalano, Deborah Chilà, Giuseppe Antonio Pablo Cirrone, Tommaso Croci, Giacomo Cuttone, Giampiero De Cesare, *Member, IEEE*, Sylvain Dunand, Michele Fabi, Luca Frontini, Catia Grimani, Maria Ionica, Keida Kanxheri, Matthew Large, Valentino Liberali, Nicola Lovecchio, *Member, IEEE*, Maurizio Martino, Giuseppe Maruccio, Giovanni Mazza, Anna Grazia Monteduro, Arianna Morozzi, *Member, IEEE*, Francesco Moscatelli, Augusto Nascetti, *Member, IEEE*, Stefania Pallotta, Andrea Papi, Daniele Passeri, *Senior Member, IEEE*, Maddalena Pedio, Marco Petasecca, *Member, IEEE*, Giada Petringa, Francesca Peverini, Lorenzo Piccolo, Pisana Placidi, *Senior Member, IEEE*, Gianluca Quarta, Silvia Rizzato, Giulia Rossi, Federico Sabbatini, Leonello Servoli, Alberto Stabile, Cinzia Talamonti, Jonathan Emanuel Thomet, Luca Tosti, Mattia Villani, Richard J. Wheadon, Nicolas Wyrsch, and Nicola Zema

***Abstract*—Hydrogenated amorphous silicon (a-Si:H) is a material having an intrinsically high radiation hardness that can be deposited on flexible substrates such as polyimide (PI). For these properties, a-Si:H can be used for the production of flexible sensors. a-Si:H sensors can be successfully utilized in dosimetry, beam monitoring for particle physics (X-ray, electron, gamma ray, and proton detection) and radiotherapy, radiation flux measurement for space applications (study of solar energetic particles and stellar events), and neutron flux measurements. In this article, we have studied the dosimetric X-ray response of n-i-p diodes deposited on PI. We measured the linearity of the photocurrent response to X-rays versus dose rate from which we have extracted the dosimetric X-ray sensitivity at various bias voltages. In particular, low bias voltage operation has been studied to assess the high energy efficiency of these kinds of sensors. A measurement of stability of X-ray response versus time has been shown. The effect of detectors annealing has been studied. Operation under bending at various bending radii is also shown.**

***Index Terms*— Flexible detectors, hydrogenated amorphous silicon (a-Si:H) detectors, radiation detectors.**

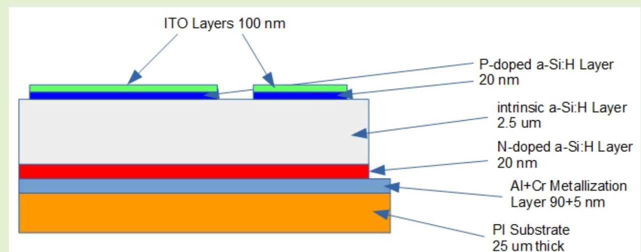

Manuscript received 30 September 2023; revised 21 December 2023; accepted 3 January 2024. Date of publication 22 February 2024; date of current version 16 April 2024. This work was supported in part by the Hydrogenated Amorphous Silicon PIxel DEtector (HASPIDE) project of National Institute of Nuclear Physics (INFN) through Commissione Nazionale Scientifica n.5 (CSN5) and in part by the "Fondazione Cassa di Risparmio di Perugia" through the RIvelatori al Silicio Amorfo Idrogenato (RISAI) Project under Grant 2019.0245. The work of Luca Antognini and Jonathan Emanuel Thomet was supported by the Swiss National Science Foundation under Grant 200021_212208/1. The work of Aishah Bashiri was supported by Najran University, Saudi Arabia. The work of Matthew Large was supported in part by the Australian Government Research Training Program (AGRTP) Scholarship and in part by the Australian Institute of Nuclear Science (AINSE) Post-Graduate Research Award (PGRA). The work of Francesca Peverini was supported by the Programma Operativo Nazionale (PON) Program through the Ph.D. Scholarship. The associate editor coordinating the review of this article and approving it for publication was Dr. Prasanta Guha. *(Corresponding author: Mauro Menichelli.)*

Please see the Acknowledgment section of this article for the author affiliations.

Digital Object Identifier 10.1109/JSEN.2024.3359861

I. Introduction

HYDROGENATED amorphous silicon (a-Si:H) is a disordered semiconductor that can be deposited by plasma-enhanced chemical vapor deposition (PECVD) from a mixture of silane (SiH_4) and hydrogen at typical temperatures of 180 °C–250 °C. Plasma excitation for the material used to fabricate the sensors described in this article is performed using VHF at 70 MHz [1]. Due to the low deposition temperature of a-Si:H, it can be easily deposited on flexible materials such as polyimide (PI). The disordered nature of a-Si:H also includes the presence of dangling bonds. In pure amorphous silicon, these dangling bonds lead to a highly defective material. However, the passivation process by hydrogenation allows the reduction, by several orders of magnitude, of the density of the defects and also increases the bandgap. This results in making a-Si:H a viable material for radiation detector

1558-1748 © 2024 IEEE. Personal use is permitted, but republication/redistribution requires IEEE permission.
See https://www.ieee.org/publications/rights/index.html for more information.
Authorized licensed use limited to: CNR Biblioteca Centrale. Downloaded on July 02,2024 at 09:21:48 UTC from IEEE Xplore. Restrictions apply.

fabrication, solar cell production, and also for the development of electronic devices [2], [3].

Another relevant feature of a-Si:H is its excellent radiation resistance. Photons [4], [5], protons [6], and recently also neutrons [7] radiation tests have been performed on a-Si:H solar cells and detectors. The results of photon and proton tests are summarized in [8].

The HASPIDE project [9] is devoted to the development of flexible and low power consumption a-Si:H sensors deposited on PI having either an n-i-p diode structure or charge-selective contact (CSC) device structure [10]. The main application foreseen for these sensors includes beam monitoring for high-energy physics applications and clinical beams, and as TRansmission Detectors (TRDs) both for electron beams for radiotherapy and proton accelerators for hadron therapy. Additional interesting fields of application for these sensors include X-ray beam dose profiling for medical and industrial applications [11], detectors for solar flare events monitoring to be used in space missions [12], and neutron detection for industrial, nuclear safeguard, and homeland security.

For these applications, flexibility is mostly important for on-body applications in medical dosimetry where a bendable detector can be directly applied on the patient body making a more precise dose evaluation. Another application where bending is important is the usage of this detector in the vacuum-to-air separation membrane of accelerator's lines, which can be made of PI and is usually bent toward the vacuum side; in this case, this detector can be used as a beam profile monitor at extraction flange, and in this case, the detector can be directly deposited on the membrane itself. Concerning beam monitoring a thin and flexible detector can also be used for direct monitoring of environmental radiation, beam quality, or residual radiation in radiation facilities for ions, photons, or electrons. In the field of cultural heritage, a flexible X-ray (or neutron detector coupling this sensor with a converter) detector can allow in situ direct analyses for bulky nonflat objects and nondestructive structural characterization under multiple radiation sources.

In this article, the X-ray response of 5 × 5 mm and 2 × 2 mm n-i-p diodes both having 2.5 μm thickness is reported. Both sizes of diodes have been studied for leakage current versus biasing voltage. Also, the photocurrent at various dose rates has been studied in order to extract the radiation sensitivity of devices at various bias voltages, including very low voltages (0–1 V). Preliminary annealing effects and long-term (about 6 h) stability of response measurements have been performed and the operation of bent detectors has also been tested.

II. X-Ray Response of n-i-p Diodes on PI

The radiation sensors for the HASPIDE project have two different configurations n-i-p diodes and CSC devices. The n-i-p diodes are formed by a thin (e.g., tens of nanometers) layer of p-doped a-Si:H, a thicker (1–10 μm) layer of intrinsic (undoped) a-Si:H, and a thin layer of n-type doped a-Si:H. CSC devices [10] are based on a three-layer structure featuring a thin layer of metal oxides where, with a small activation energy (such as TiO_2), a thick layer of intrinsic a-Si:H, and a thin layer of metal oxides with a large activation energy (such as MoO_x or WO_x). In this article, tests on n-i-p diodes will be shown. The detailed structure of this device is shown in Fig. 1. On the top of a 25-μm-thick PI substrate, an aluminum layer is deposited via sputtering (90 nm thickness). In order to avoid diffusion of aluminum in a-Si:H, a layer of 5 nm of chromium is deposited over the aluminum using the same technique. On top of this metal, a layer of n-doped a-Si:H is deposited (ca. 20 nm thickness) via PECVD from a mixture of SiH_4, H_2, and PH_3. To create an n-i-p structure, a 2.5-μm layer of intrinsic a-Si:H is deposited on top of the n-doped layer (via PECVD). On top of this layer, a patterned deposition of p-doped a-Si:H is performed (PECVD of a mixture of SiH_4, H_2, and B_2H_4). On the p-doped pattern, a deposition of indium tin oxide (ITO) is performed via sputtering; a top view of the resulting detector is shown in Fig. 2.

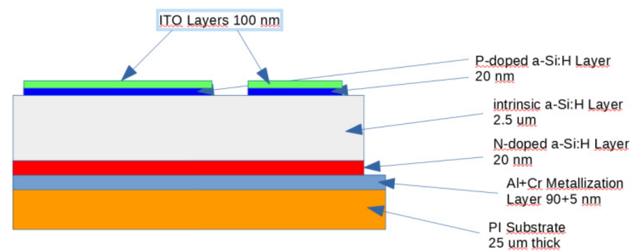

Fig. 1. Layout of HASPIDE n-i-p diode prototype.

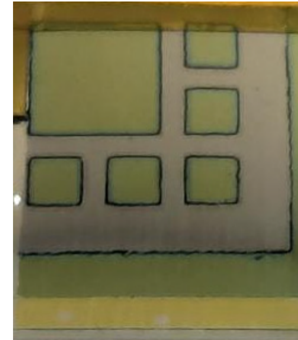

Fig. 2. Picture from the top of the detector array before packaging. One 5 × 5 mm device and five 2 × 2 mm devices are deposited on PI. The light green area is the ITO contacts, the gray area is the intrinsic a-Si:H, and the gray area below the green-yellow area is the Cr + Al back contact.

The X-ray setup used for the measurements described in this article is shown in Fig. 3. The irradiated sample includes five 2 × 2 mm and one 5 × 5 mm n-i-p diodes and is glued and bonded (using a copper-based conductive glue) to a printed circuit board (PCB) frame. This is connected to an interface board in connection with a Keithley 2400 source measuring unit (SMU) that is used for biasing the sensor and measuring the output current with a resolution of about 1 pA. The sensor is exposed to X-rays generated by a 10-W X-ray tube from Newton Scientific operating at 50-kV maximum voltage and 200-μA maximum current [13].

Fig. 4 shows the measurements of dark current at room temperature versus voltage for a 2 × 2 mm (small diode) and for a 5 × 5 mm (large diode) sensor. The power absorption at 1 V of the detector is 10 pW (large diode) and 1 pW (small

Authorized licensed use limited to: CNR Biblioteca Centrale. Downloaded on July 02,2024 at 09:21:48 UTC from IEEE Xplore. Restrictions apply.

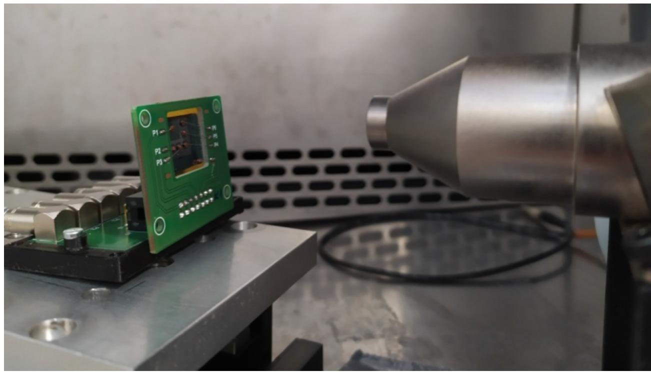

Fig. 3. Setup for X-ray testing. The detector shown in Fig. 2 is connected to the SMU through a PCB interface frame. The picture also shows the X-ray tube collimator. The entire setup is enclosed in a climatic chamber for temperature stabilization.

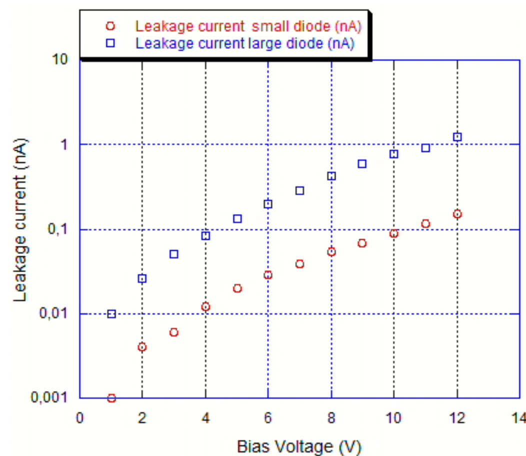

Fig. 4. Leakage current at room temperature versus bias voltage for the 2 × 2 mm device (small diode) and for the 5 × 5 mm device (large diode).

diode) while at 10 V bias is below 10 nW for a large diode and 1 nW for a small diode. The ratio between the leakage currents of the large and the small diode is approximately equal to the ratio of the sensor areas.

In order to measure dosimetric sensitivity, the detectors have been irradiated with X-rays using a tube voltage of 40 kV in the range from about 20 to 200 μA of tube current. The dose rate of the emitted radiation in this setup was measured according to the procedure shown in [7]. The large and the small sensors were irradiated in the dose rate range from 0.36 to 3.11 cGy/s and the photocurrents have been measured at different values of the detector bias. After the subtraction of the leakage current, the photocurrent has been plotted versus X-ray tube emitted dose rate at various bias voltages and the results are plotted in Fig. 5 for the large diode and in Fig. 6 for one small diode. From these figures, it is possible to infer the very good linearity of the detector responses in the measured range.

The dosimetric sensitivities and linear regression coefficients have been extracted from the slopes of the lines coming from the linear fit; these calculated quantities are shown in Table I.

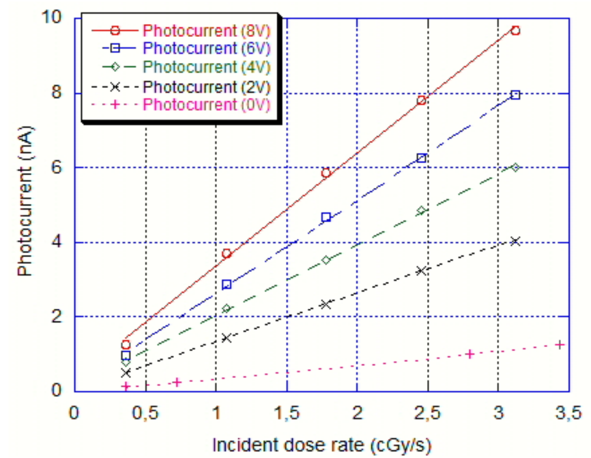

Fig. 5. Net photocurrent versus incident X-ray dose rate for the large (5 × 5 mm) device at various bias voltages.

TABLE I
DOSIMETRIC SENSITIVITY VALUES AND LINEAR REGRESSION COEFFICIENTS

Device Area (mm^2)	Bias Voltage	Dosimetric sensitivity (nC/cGy)	Regression coefficient R
5 x 5	0V	0.367	0.99999
	2V	1.283	0.99991
	4V	1.900	0.99975
	6V	2.505	0.99972
	8V	3.027	0.99926
2 x 2	1V	0.137	0.99878
	4V	0.335	0.99961
	8V	0.540	0.99881

From these measurements, it is possible to determine the power consumption under irradiation. For the small diode at 1-V bias, the absorbed power ranges from 54 pW at 0.36 cGy/s to 432 pW at 3.11 cGy/s, while at 8 V, it ranges from 2.74 to 14.76 nW. For the large diode, also the photocurrent at 0V bias has been measured with negligible power consumption while at 8 V the power consumption of the detector ranges from 10.24 nW to 77.36 nW. These data demonstrate the very low power consumption of these sensors.

III. LONG-TERM STABILITY OF N-I-P DEVICES MEASURED WITH X-RAYS

A test on the longer term of the X-ray response of these devices has also been performed: a 5 × 5 mm device has been irradiated for 2.1 × 10^4 s at 40-kV tube bias voltage with a dose rate of 0.4 cGy/s. Fig. 7 shows the raw data of the time profile of the collected photocurrent (red data points), and the slow rise of the current, in the stabilization phase, may be due to thermal effects. For this reason, a background dark current, evaluated by a linear extrapolation between the dark current before and after irradiation, has been subtracted from the raw photocurrent. The result of this correction is shown with the green data points. After the application of this algorithm, we are able to compensate for the thermal effect of the X-ray irradiation.

Authorized licensed use limited to: CNR Biblioteca Centrale. Downloaded on July 02,2024 at 09:21:48 UTC from IEEE Xplore. Restrictions apply.

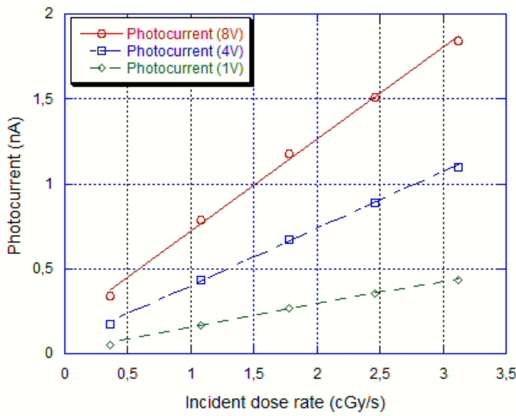

Fig. 6. Net photocurrent versus incident X-ray dose rate for the small (2 × 2 mm) device at various bias voltages.

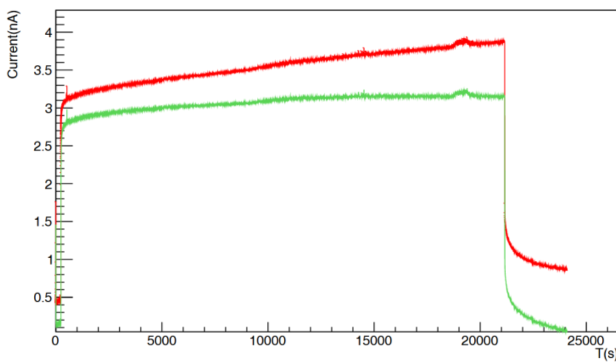

Fig. 7. Raw photocurrent of a 5 × 5 mm n-i-p device biased at 8 V and irradiated at the rate of 0.4 cGy/s versus time (red data points) and photocurrent corrected for the increase of background leakage current due to thermal effect (green data points).

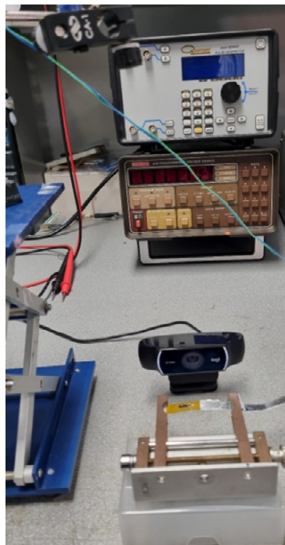

Fig. 8. Setup for the bending test. The sample is glued on a Kapton PCB shielded by aluminum. The support is mounted on a jig with two jaws to change the bending radius. The camera and the laser diode (on the top) are also shown.

IV. Operation of the Sensor During Bending

In order to test the operation of the device when bent, a bending test has been performed on the sensor using a 615-nm optical laser. The test setup is shown in Fig. 8. The detector is glued on a flexible PI PCB support; the support is fixed on a jig equipped with two jaws that, approaching each other, cause the curvature of the support and, therefore, of the sensor. A camera observes the support from the side, and using appropriate software (ImageJ [14]), it is possible to superimpose a circle on the bent support image and calculate the radius of curvature of the bending (Fig. 9). By illuminating the sensor with the laser, the photocurrent has been measured on the sensor, to check whether there are relevant changes due to bending. The laser is mounted on movable support in order to keep the same distance from the sensor to correct for the small divergence. The measurement started from a flat configuration of the support and the measured value was used for the photocurrent measurements taken during bending. The curvature was then increased to a bending radius of about 8 mm and then decreased back again to a flat position. The results of the relative photocurrent versus curvature radius are shown in Fig. 10(a). The points on the blue line were taken during a bending radius decrease and the points on the brown

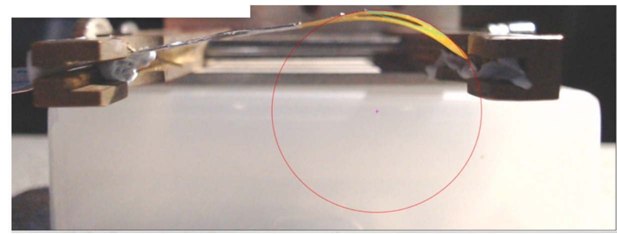

Fig. 9. Bent sensor on the jig and the curvature radius measurement.

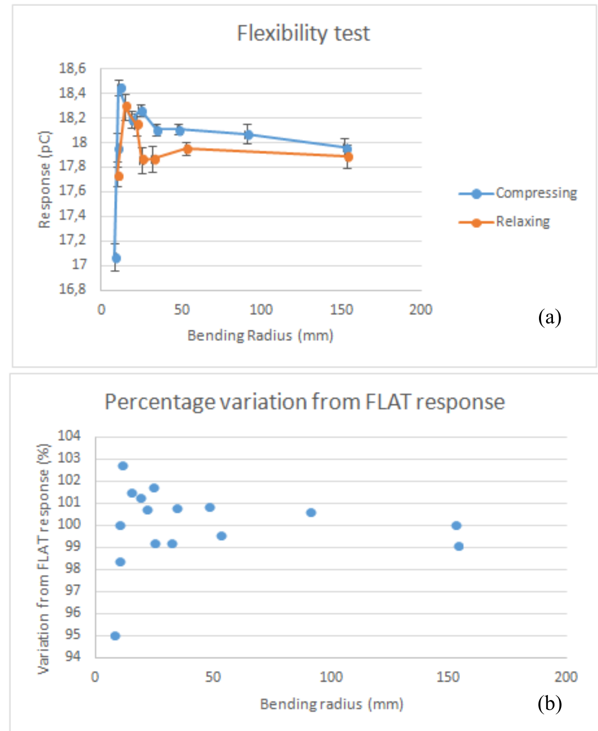

Fig. 10. Results from bending measurements. (a) Charge response versus bending radius. Measurements on the blue line are taken during compression and measurements on the brown line are taken during relaxation. (b) Deviation from flat response (100%) versus bending radius.

Authorized licensed use limited to: CNR Biblioteca Centrale. Downloaded on July 02,2024 at 09:21:48 UTC from IEEE Xplore. Restrictions apply.

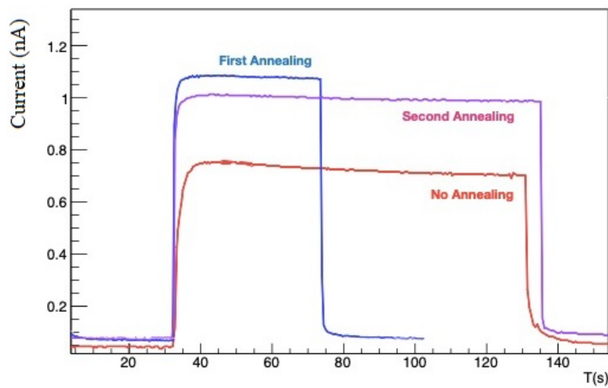

Fig. 11. Photocurrent amplitude signal of an a-Si:H sensor before annealing (orange line) and after 12 h of annealing (blue line) and 24 h of annealing (purple line).

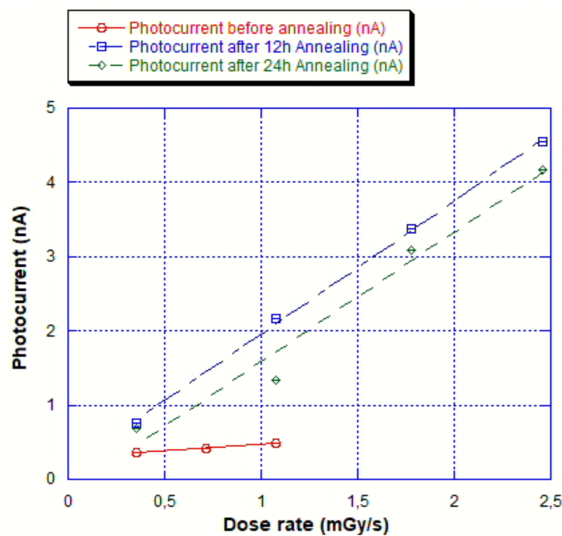

Fig. 12. Photocurrent versus dose rate response of a fresh detector (red line and dots), 12-h annealed (blue dot and line), and 24-h annealed device (green dot and line).

line were taken during a bending radius increase, in order to check for degradation or hysteresis; Fig. 10(b) shows the percentage of the deviation from the initial photocurrent.

From the measurements, we can see that except for the point at an 8-mm bending radius, where the photocurrent is 95% of the flat response, the deviation from the flat response is below 3% and there is only a little difference between response during curvature radius decrease (compression) and response during curvature radius increase (relaxation).

V. Annealing Studies

During radiation damage tests with neutrons [7] especially at 10^{16} n_{eq}/cm^2 for n-i-p devices, a very large recovery effect due to annealing has been observed. The irradiated components, after the annealing, improved their characteristics not only in comparison with the post-irradiation phase but also in comparison to the performances measured before irradiation. For these reasons, we tested nonirradiated components before and after annealing. The annealing was performed in two phases: 1) 12 h of baking at 100 °C and 2) 24 h (overall) of baking at 100 °C. Fig. 11 shows the photocurrent versus time, where at an irradiation of 2.456 mGy/s, we can notice the time response of the various stages of the annealing test. Fig. 12 shows the photocurrent versus X-ray dose rate for the component after the first and second phases of the annealing test. From this graph, we can notice a large increase in the dosimetric sensitivity response (from 1.8 to 18.0 nC/cGy) after the first phase, while after the second phase, a small decrease in the response is observed (from 18.0 to 17.4 nC/cGy).

From this test, we can infer that annealing can be beneficial not only on irradiated components but also on nonirradiated ones. Although the best duration for this annealing is still under optimization, these results suggest that it will be below 12 h.

VI. Conclusion

Two different size (2 × 2 mm and 5 × 5 mm) a-Si:H n-i-p devices on PI (having 2.5 μm thickness) have been built in the context of the HASPIDE project, aiming at the construction of flexible planar detectors for radiation flux measurements and neutron detection. These devices have been tested for leakage current, dosimetric sensitivity at various bias voltages, long-term behavior in response, flexibility, and annealing. The results show a very good linearity in the dose rate range tested, in addition to a good sensitivity and leakage current scaling with the area of the devices. Power requirements of the detectors range from tens of picowatts to tens of nanowatts depending on sensor size and bias voltage. Bias voltage is related to the dosimetric sensitivity of the device; the greater the needed sensitivity, the higher the bias voltage required, and therefore, a higher power consumption is expected. The long-term behavior of the sensor is sufficiently stable especially whether power dissipation is correctly implemented. Flexibility under operation is very good; above 1 cm of bending radius, the photocurrent variations are contained within ±3% of the flat-sensor response. Furthermore, we observe a beneficial effect on the device annealed for 12 h at the temperature of 100 °C.

Acknowledgment

Mauro Menichelli, Mirco Caprai, Maria Ionica, Arianna Morozzi, Andrea Papi, Leonello Servoli, and Luca Tosti are with the National Institute of Nuclear Physics (INFN), 06123 Perugia, Italy (e-mail: Mauro.menichelli@pg.infn.it).

Luca Antognini, Sylvain Dunand, Jonathan Emanuel Thomet, and Nicolas Wyrsch are with the Institute of Electrical and Microengineering (IME), Ecole Polytechnique Fédérale de Lausanne (EPFL), 2000 Neuchâtel, Switzerland.

Saba Aziz, Lucio Calcagnile, Anna Paola Caricato, Maurizio Martino, Giuseppe Maruccio, Anna Grazia Monteduro, Gianluca Quarta, and Silvia Rizzato are with the National Institute of Nuclear Physics (INFN) and the Dipartimento di Matematica e Fisica, Università del Salento, 73100 Lecce, Italy.

Aishah Bashiri is with the Centre for Medical Radiation Physics, University of Wollongong, Wollongong, NSW 2522, Australia, and also with the Department of Physics, Najran University, Najran 11001, Saudi Arabia.

Marco Bizzarri, Keida Kanxheri, Francesca Peverini, and Giulia Rossi are with the National Institute of Nuclear Physics (INFN), 06123 Perugia, Italy, and also with the Dipartimento di Fisica e Geologia, Università degli Studi di Perugia, 06123 Perugia, Italy.

Domenico Caputo, Giampiero De Cesare, and Nicola Lovecchio are with the INFN Sezione di Roma, 00185 Rome, Italy, and also with the Dipartimento Ingegneria dell'Informazione, Elettronica e Telecomunicazioni, Università degli Studi di Roma, 00184 Rome, Italy.

Authorized licensed use limited to: CNR Biblioteca Centrale. Downloaded on July 02,2024 at 09:21:48 UTC from IEEE Xplore. Restrictions apply.

Roberto Catalano, Giuseppe Antonio Pablo Cirrone, Giacomo Cuttone, and Giada Petringa are with the INFN Laboratori Nazionali del Sud, 95123 Catania, Italy.

Deborah Chilà, Stefania Pallotta, and Cinzia Talamonti are with the INFN Sezione di Firenze, 50019 Sesto Fiorentino, Italy, and also with the Department of Experimental and Clinical Biomedical Sciences "Mario Serio," University of Florence, 50135 Florence, Italy.

Tommaso Croci, Daniele Passeri, and Pisana Placidi are with the National Institute of Nuclear Physics (INFN), 06123 Perugia, Italy, and also with the Dipartimento di Ingegneria, Università degli Studi di Perugia, 06125 Perugia, Italy.

Michele Fabi, Catia Grimani, Federico Sabbatini, and Mattia Villani are with the INFN Sezione di Firenze, 50019 Sesto Fiorentino, Italy, and also with the Dipartimento di Scienze Pure e Applicate, Università di Urbino Carlo Bo, 61029 Urbino, Italy.

Luca Frontini, Valentino Liberali, and Alberto Stabile are with the INFN Sezione di Milano, 20133 Milan, Italy.

Matthew Large and Marco Petasecca are with the Centre for Medical Radiation Physics, University of Wollongong, Wollongong, NSW 2522, Australia.

Giovanni Mazza, Lorenzo Piccolo, and Richard J. Wheadon are with the INFN Sezione di Torino, 10125 Turin, Italy.

Francesco Moscatelli and Maddalena Pedio are with the National Institute of Nuclear Physics (INFN), 06123 Perugia, Italy, and also with CNR-IOM, 06123 Perugia, Italy.

Augusto Nascetti is with the INFN Sezione di Roma, 00185 Rome, Italy, and also with the Scuola di Ingegneria Aerospaziale, Università degli Studi di Roma, 00138 Rome, Italy.

Nicola Zema is with the National Institute of Nuclear Physics (INFN), 06123 Perugia, Italy, and also with the CNR Istituto struttura della Materia, 00133 Rome, Italy.

References

[1] N. Wyrsch and C. Ballif, "Review of amorphous silicon based particle detectors: The quest for single particle detection," *Semicond. Sci. Technol.*, vol. 31, no. 10, Oct. 2016, Art. no. 103005.

[2] H. C. Tuan, "Amorpiious silicon thin film transistor and its applications to large-area electrionics," *MRS Proc.*, vol. 33, pp. 247–257, 1984.

[3] A. E. Owen, P. G. Le Comber, W. E. Spear, and J. Hajto, "Memory switching in amorphous silicon devices," *J. Non-Crystalline Solids*, vols. 59–60, pp. 1273–1280, Dec. 1983.

[4] J. R. Srour et al., "Damage mechanisms in radiation-tolerant amorphous silicon solar cells," *IEEE Trans. Nucl. Sci.*, vol. 45, no. 6, pp. 2624–2631, Dec. 1998.

[5] J. M. Boudry and L. E. Antonuk, "Radiation damage of amorphous silicon photodiode sensors," *IEEE Trans. Nucl. Sci.*, vol. 41, no. 4, pp. 703–707, Aug. 1994.

[6] N. Wyrsch et al., "Radiation hardness of amorphous silicon particle sensors," *J. Non-Crystalline Solids*, vol. 352, nos. 9–20, pp. 1797–1800, Jun. 2006.

[7] M. Menichelli et al., "Neutron irradiation of hydrogenated amorphous silicon p-i-n diodes and charge selective contacts detectors," *Nucl. Instrum. Methods Phys. Res. A, Accel. Spectrom. Detect. Assoc. Equip.*, vol. 1052, Jul. 2023, Art. no. 168308.

[8] M. Menichelli, L. Servoli, and N. Wyrsch, "Status and perspectives of hydrogenated amorphous silicon detectors for MIP detection and beam flux measurements," *Frontiers Phys.*, vol. 10, Oct. 2022, Art. no. 943306.

[9] M. Menichelli et al., "Development of thin hydrogenated amorphous silicon detectors on a flexible substrate," 2022, *arXiv:2211.17114*.

[10] M. Menichelli et al., "Testing of planar hydrogenated amorphous silicon sensors with charge selective contacts for the construction of 3D-detectors," *J. Instrum.*, vol. 17, no. 3, Mar. 2022, Art. no. C03033.

[11] M. J. Large et al., "Hydrogenated amorphous silicon high flux X-ray detectors for synchrotron microbeam radiation therapy," *Phys. Med. Biol.*, vol. 68, no. 13, Jul. 2023, Art. no. 135010, doi: 10.1088/1361-6560/acdb43.

[12] C. Grimani et al., "A hydrogenated amorphous silicon detector for space weather applications," 2023, *arXiv:2302.00339*.

[13] *Datasheet*. Accessed: Sep. 18, 2023. [Online]. Available: http://www.newtonscientificinc.com/50kv-10w-monoblock/

[14] *ImageJ Software and Related Documentation*. Accessed: Sep. 18, 2023. [Online]. Available: https://imagej.net/ij/index.html last

Authorized licensed use limited to: CNR Biblioteca Centrale. Downloaded on July 02,2024 at 09:21:48 UTC from IEEE Xplore. Restrictions apply.